

# MIPAS measurements of upper tropospheric C<sub>2</sub>H<sub>6</sub> and O<sub>3</sub> during the southern hemispheric biomass burning season in 2003

T. v. Clarmann<sup>1</sup>, N. Glatthor<sup>1</sup>, M. E. Koukouli<sup>2</sup>, G. P. Stiller<sup>1</sup>, B. Funke<sup>3</sup>, U. Grabowski<sup>1</sup>, M. Höpfner<sup>1</sup>, S. Kellmann<sup>1</sup>, A. Linden<sup>1</sup>, M. Milz<sup>1,\*</sup>, T. Steck<sup>1,\*\*</sup>, and H. Fischer<sup>1</sup>

<sup>1</sup>Forschungszentrum Karlsruhe, Institut für Meteorologie und Klimaforschung Karlsruhe, Germany

<sup>2</sup>Laboratory of Atmospheric Physics, Physics Department, Aristotle University of Thessaloniki, Thessaloniki, Greece.

<sup>3</sup>Instituto de Astrofísica de Andalucía CSIC, Granada, Spain

\* now at: Institutionen för Rymdvetenskap, Luleå Tekniska Universitet, Kiruna, Sweden

\*\* now at: Kepler Gymnasium, Ulm, Germany

Received: 26 July 2007 – Published in Atmos. Chem. Phys. Discuss.: 15 August 2007

Revised: 24 October 2007 – Accepted: 13 November 2007 – Published: 27 November 2007

**Abstract.** Under cloud free conditions, the Michelson Interferometer for Passive Atmospheric Sounding (MIPAS) provides measurements of spectrally resolved limb radiances down to the upper troposphere. These are used to infer global distributions of mixing ratios of atmospheric constituents in the upper troposphere and the stratosphere. From 21 October to 12 November 2003, MIPAS observed enhanced amounts of upper tropospheric C<sub>2</sub>H<sub>6</sub> (up to about 400 pptv) and ozone (up to about 80 ppbv). The absolute values of C<sub>2</sub>H<sub>6</sub>, however, may be systematically low by about 30% due to uncertainties of the spectroscopic data used. By means of trajectory calculations, the enhancements observed in the southern hemisphere are, at least partly, attributed to a biomass burning plume, which covers wide parts of the Southern hemisphere, from South America, the Atlantic Ocean, Africa, the Indian Ocean to Australia. The chemical composition of the part of the plume-like pollution belt associated with South American fires, where rainforest burning is predominant appears different from the part of the plume associated with southern African savanna burning. In particular, African savanna fires lead to a larger ozone enhancement than equatorial American fires. In this analysis, MIPAS observations of high ozone were disregarded where low CFC-11 (below 245 pptv) was observed, because this hints at a stratospheric component in the measured signal. Different type of vegetation burning (flaming versus smouldering combustion) has been identified as a candidate explanation for the different plume compositions.

## 1 Introduction

Long-lived products of biomass burning are intercontinentally transported and form large plume-like structures which are visible over months. The Atmospheric Chemistry Experiment (ACE) has measured CO, C<sub>2</sub>H<sub>6</sub>, HCN and C<sub>2</sub>H<sub>2</sub> during the 2004 and 2005 southern hemispheric biomass burning seasons (Rinsland et al., 2005; Coheur et al., 2007). The Measurements Of Pollution In The Troposphere (MOPITT) experiment has provided evidence of enhanced tropospheric CO in the outflow regions of African and South American forest fires during the 2003 southern hemispheric biomass burning season as recently published by Edwards et al. (2006). The Michelson Interferometer for Passive Atmospheric Sounding (MIPAS) instrument provides a complementary dataset of this episode, namely upper tropospheric C<sub>2</sub>H<sub>6</sub> and ozone volume mixing ratios in October–November 2003. These data contribute additional information on tropical latitudes which are not as well covered by the ACE instrument, and adds to the knowledge of the chemical composition of the polluted air detected by MOPITT. C<sub>2</sub>H<sub>6</sub> is a direct biomass burning product generated predominantly by smouldering combustion (Lobert and Warnatz, 1993), while O<sub>3</sub> is a secondary biomass burning product generated by photochemistry in the presence of NO<sub>x</sub>. To our knowledge, our data are the first global upper tropospheric C<sub>2</sub>H<sub>6</sub> data set which also densely covers tropical latitudes.

While the term “plume” typically is associated with the outflow of a single source, in the context of biomass burning this term is occasionally used also for contiguous outflow patterns of multiple sources (e.g. Chatfield et al., 2002). The latter authors also use the terms “global plume” or “megaplume”. For simplicity, we use the term “plume” also in the context of multiple sources in this paper.

Correspondence to: T. von Clarmann  
(thomas.clarmann@imk.fzk.de)

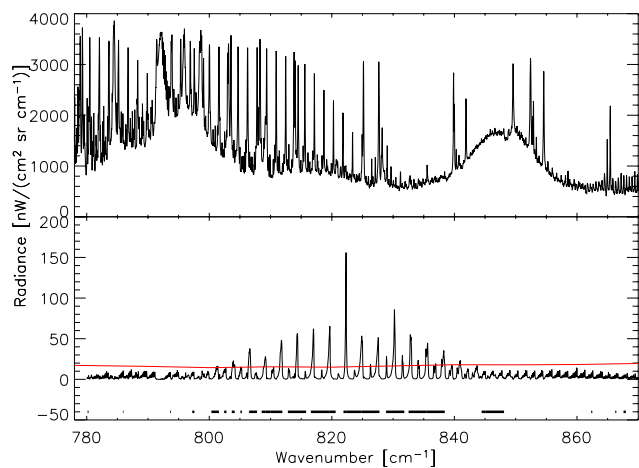


**Fig. 1.** MIPAS spectrum in the wavenumber range where C<sub>2</sub>H<sub>6</sub> is analysed, measured at 13.0° S, 37.2° E on 21 October 2003, 10.06 km tangent altitude (upper panel). The lower panel is the C<sub>2</sub>H<sub>6</sub> signal, determined by subtracting a calculated spectrum with zero C<sub>2</sub>H<sub>6</sub> in the target altitude region (8–12 km) from the best fitting calculated spectrum. Microwindows are indicated as horizontal bars. The horizontal red line is the noise equivalent spectral radiance of a single spectrum.

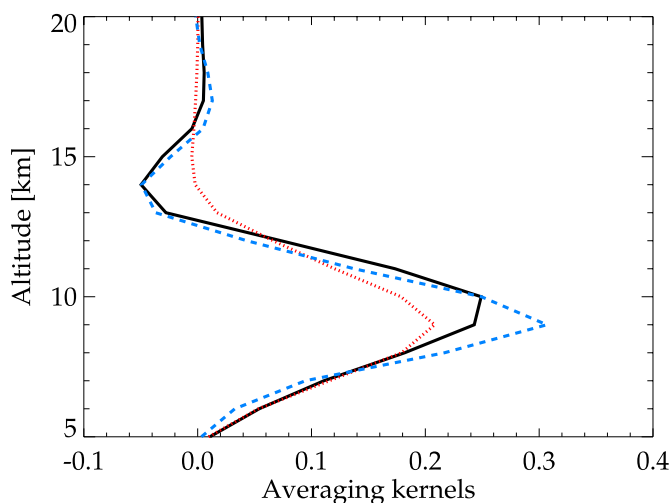


**Fig. 2.** Rows of averaging kernels at 9 km altitude for C<sub>2</sub>H<sub>6</sub> (black, solid), O<sub>3</sub> (red, dotted), and CFC-11 (blue, dashed) for a profile measured on 21 October 2003 at 13.0° S, 37.2° E.

## 2 MIPAS observations

MIPAS (Michelson Interferometer for Passive Atmospheric Sounding) is part of the instrumentation of the Environmental Satellite (Envisat) which was launched into its sun-synchronous polar orbit on 1 March 2002. It is a limb emission spectrometer designed primarily for measuring stratospheric trace species from space (Fischer et al., 2007). Nevertheless, under cloud-free conditions it also provides

information on upper tropospheric trace species. MIPAS was operational from July 2002 to March 2004 with full specification, in particular 0.05 cm<sup>-1</sup> spectral resolution in terms of full width at half maximum (apodised with the “strong” Norton and Beer (1976) function). During each of the 14.4 orbits per day MIPAS recorded 78 limb sequences of emission spectra, amounting at about 1000 observations per day from pole to pole. Full global coverage is achieved after 3 days. Data presented here were recorded from 21 October to 12 November 2003, during Envisat orbits 8573 to 8931. The data analysis reported in this paper relies on the ESA-provided so-called level-1B data product version 4.59 which includes calibrated phase-corrected and geolocated radiance spectra (Nett et al., 1999). Spectra containing cloud signal were identified using a method suggested by Spang et al. (2004) and have been excluded from further analysis. The general strategy and formalism of the retrieval is discussed in detail by von Clarmann et al. (2003). In the following we restrict the discussion to specific issues of the retrieval of upper tropospheric C<sub>2</sub>H<sub>6</sub> and ozone.

### 2.1 Ethane (C<sub>2</sub>H<sub>6</sub>)

Data presented in this paper are version V2.C2H6.1. Features in spectra of tangent altitudes of 33 km and lower have been analysed for C<sub>2</sub>H<sub>6</sub>. Its abundances are retrieved from the ν<sub>9</sub> fundamental emissions in the spectral region of 780–868 cm<sup>-1</sup>. In order to blank out regions with low C<sub>2</sub>H<sub>6</sub> signal and large signal of other species, 30 so-called microwindows have been selected within the analysis window (Fig. 1). Interfering species in this spectral region are O<sub>3</sub>, H<sub>2</sub>O, HNO<sub>3</sub>, ClONO<sub>2</sub>, CFC-11, ClO, N<sub>2</sub>O<sub>5</sub>, HNO<sub>4</sub>, CFC-12 and SF<sub>6</sub>, for which pre-retrieved values were used, i.e. mixing ratios retrieved in a preceding analysis step from the same set of spectra but usually different microwindows. The interferences PAN and CCl<sub>4</sub> were considered on the basis of climatological profiles, which is justified because their radiance contribution within the microwindows chosen is low. A retrieved C<sub>2</sub>H<sub>6</sub> profile has three to four degrees of freedom (i.e. independent pieces of information, calculated as the trace of the averaging kernel matrix, c.f. Rodgers, 2000), of which, at tropical geolocations where the tropopause is as high as 17 km, approximately three characterize the troposphere. Typical single profile total retrieval errors, i.e. noise and parameter errors excluding spectroscopic data uncertainties, for measurements of enhanced tropospheric C<sub>2</sub>H<sub>6</sub> vary between about 20 and 50%, depending on altitude, temperature, humidity and actual C<sub>2</sub>H<sub>6</sub> abundances. At all altitudes the error budget is dominated by measurement noise, which, from the lowest tangent altitude actually used up to 18 km, contributes an order of magnitude more than all other random error sources together. These other random errors we define are randomly varying errors due to uncertain instrumental or atmospheric parameters which might influence the retrieval, such as interfering species. The vertical resolution is about 3 to 4 km

at 9 km altitude, as determined from the row of the averaging kernel matrix (Fig. 2). Above approximately 18–20 km, the C<sub>2</sub>H<sub>6</sub> signal in the MIPAS spectra is so low that no more useful profile information can be retrieved.

A major issue with respect to the absolute accuracies of the retrieved C<sub>2</sub>H<sub>6</sub> mixing ratios are uncertainties in the spectroscopic data used (Personal communication, J. Vander Auwera, 2005; J.-M. Flaud, 2006). The line intensities in HITRAN2K (Rothman et al., 2003) which have been used for this analysis are a factor of 2 stronger than those in the GEISA spectroscopic database (Jacquinot-Husson et al., 2003), resulting in a factor of 2 lower mixing ratios. Line intensities of a more recent data set, which were not yet available at the time of this study, are about 30 percent smaller than those used here (Vander Auwerra et al., 2007). These uncertainties, however, have no impact on our conclusions since these do not depend on the absolute values retrieved. This makes our analysis robust against any scalar bias, and results can easily be re-scaled for band-intensity correction, which is a commonly used approach in atmospheric spectroscopy. The recommended correction factor to make our data set comparable to retrievals based on the new spectroscopic data by Vander Auwerra et al. (2007) is 1.292 for the spectral analysis windows used in this study.

Since the sensitivity of mid-infrared limb emission measurements to abundances of species in the troposphere is limited, data recorded between 21 October 2003 and 12 November 2003 were averaged in order to increase significance. In the following, we discuss the averaged spatial distributions of C<sub>2</sub>H<sub>6</sub> in the upper troposphere, i.e. at 275 hPa, which corresponds roughly to 9–10 km altitude. At the given altitude resolution of the vertical profiles of 3 to 4 km, assessment of adjacent altitude levels does not provide much additional information.

Widespread high C<sub>2</sub>H<sub>6</sub> mixing ratios were observed in the northern hemisphere, which is attributed to industrial pollution (Fig. 3). Values of about 200–400 pptv (260–520 pptv after application of the spectroscopic correction) were retrieved. The background mixing ratio in the southern hemisphere was only about 75 pptv (100 pptv after correction). However, there was a plume-like structure reaching from Brazil over the southern tropical Atlantic Ocean, southern Africa, the southern sub-tropical Indian Ocean to Australia and beyond. Here values of 300–400 pptv (390–520 pptv after correction) were observed, which are comparable to those in polluted airmasses in the northern hemisphere. The typical standard error of the mean mixing ratio in a longitude-latitude bin is about 30 pptv (39 pptv after correction). Volume mixing ratios measured by MIPAS are approximately a factor of 2 lower than those measured by ACE during the biomass-burning season 2004 (Rinsland et al., 2005), who used the 2976–2977 cm<sup>-1</sup> spectral region. This discrepancy is most likely to be attributed to inconsistent spectroscopic data in these two bands but is by far not removed by application of the spectroscopic correction factor. In situ

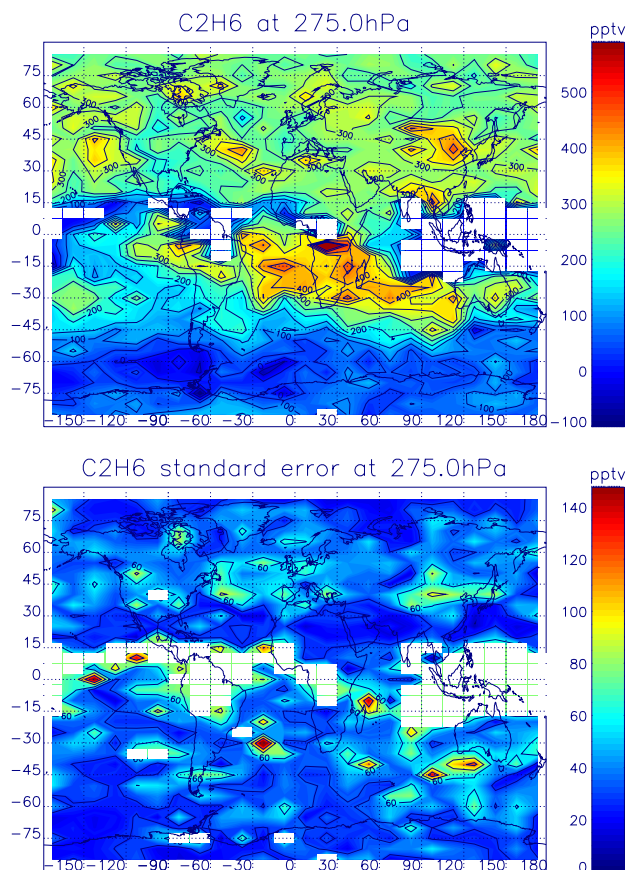


**Fig. 3.** VMR distribution of C<sub>2</sub>H<sub>6</sub> at 275 hPa, averaged from 21 October to 12 November 2003 (upper panel). Larger mixing ratios are found in the northern hemisphere, due to industrial pollution. White bins represent data gaps due to cloud coverage. In the southern hemisphere a plume-like structure is visible. The lower panel shows the standard error of the mean. Note the different colour scales. White boxes in the standard error plots represent data bins where either no data were available or only one measurement, such that the standard error could not be calculated.

measurements of about 500–700 pptv at 9 km altitude inside biomass burning plumes have been reported by Talbot et al. (1996). Although the latter measurements refer to a period in 1992, they also describe a situation of enhanced vegetation fire activity. While the original MIPAS retrievals reveal a low bias compared both to the in situ measurements and the ACE data, they agree reasonably well with the in situ data after the spectroscopic correction. While these comparisons of non-coincident data should not be overstressed, there is some indication that the spectroscopic data set by Vander Auwerra et al. (2007) is more reliable than the one included in HITRAN2K.

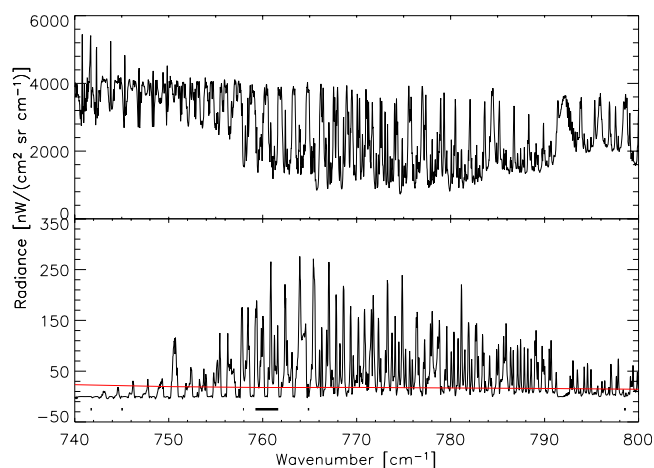


**Fig. 4.** MIPAS A band spectrum in the wavenumber range where O<sub>3</sub> is analysed. See Fig. 1 for details.

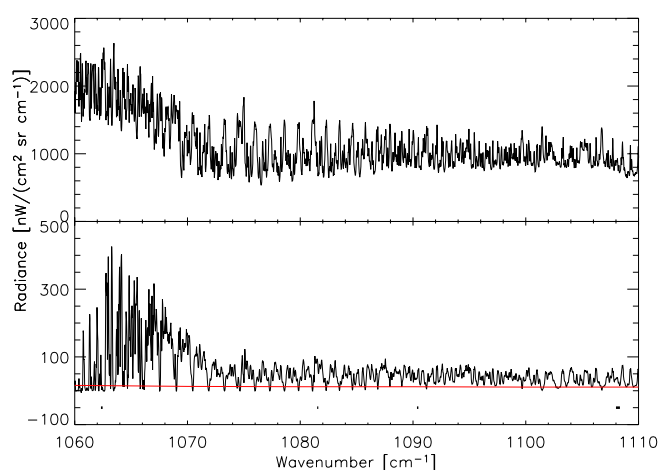


**Fig. 5.** MIPAS AB band spectrum in the wavenumber range where O<sub>3</sub> is analysed. See Fig. (1) for details.

## 2.2 O<sub>3</sub>

The ozone distributions presented in this paper are version V2\_O3\_2, and their retrieval has been described in detail in Glatthor et al. (2006). The microwindows chosen are situated both in the MIPAS A band (685–970 cm<sup>-1</sup>) and AB band (1020–1170 cm<sup>-1</sup>) (Fig. 4 and 5). Detailed validation is presented by Steck et al. (2007b). Under tropical enhanced tropospheric ozone conditions, the retrieval has 2 to 3 degrees of freedom in the troposphere. Typical estimated single profile retrieval errors are of the order of 50% or more for upper tropospheric background concentrations but are reduced to reasonable values by averaging over the observation period within latitude-longitude bins (see Sect. 2.1). At tropospheric altitudes the error budget is dominated by measurement noise, followed by uncertainties in spectral shift and temperature. The altitude resolution at 9 km altitude, as determined from the rows of the averaging kernel matrix (Fig. 2), is about 4 km. The uncertainty of spectroscopic data varies from 2–10%, depending on the particular band and rotational quantum number. For the transitions used here, 5% is considered a representative estimate. The standard error of the mean ozone mixing ratio over the analysis period in a latitude-longitude bin of enhanced ozone is of the order of 3 ppbv.

O<sub>3</sub> abundances at 275 hPa are high towards polar latitudes where stratospheric air is seen (Fig. 6). Towards the tropics, values of only 0–50 ppbv were observed both in northern and southern low latitudes. Higher values of up to 80 ppbv are confined to a subset of the latitude-longitude bins where also enhanced C<sub>2</sub>H<sub>6</sub> was observed. No coincident tropospheric O<sub>3</sub> data from other satellite instruments have been found to compare with. Comparison to tropospheric ozone maps generated with the empirically corrected tropospheric ozone residual (TOR) technique from solar backscattered

ultraviolet (SBUV) data for September through November 1979–2000 (Fishman et al., 2003) (their Fig. 1) reveals similarities in the distribution of enhanced O<sub>3</sub> over the southern Atlantic Ocean, Africa, and Indian Ocean, while their TOR ozone data show enhanced ozone also above South America. This difference, however, should not be overstressed, because TOR data also represent the lower troposphere which is not seen by MIPAS, and because the mean distributions are based on different measurement periods, which cover the local biomass burning season differently. In particular, major fire activities seem to have taken place in Brazil after the MIPAS averaging period.

## 2.3 CFC-11

In this study the volume mixing ratio of CFC-11 is used as an indicator to distinguish between tropospheric and stratospheric air. CFC-11 is retrieved in the 838.0–853.0 cm<sup>-1</sup> spectral region, which covers the ν<sub>4</sub> band (Fig. 7). Main interfering lines in this region are associated to H<sub>2</sub>O, HNO<sub>3</sub> and COCl<sub>2</sub>. In order to avoid propagation of uncertainties of a priori knowledge on these species to the CFC-11 profiles, their abundances are joint-fitted in the CFC-11-analysis window. The estimated total retrieval error of tropospheric CFC-11 is only 4–9% except for particularly moist atmospheric conditions where enhanced opacity of the atmosphere due to water vapour emissions or even undetected thin clouds affect the retrieval. Besides this, the main component of the CFC-11 retrieval error is line-of-sight uncertainties, which even outweigh the contribution of measurement noise. The altitude resolution is about 3.3 km. The tropical troposphere is characterized by three to four degrees of freedom of the retrieved CFC-11 profile. A dedicated paper on the retrieval of CFC-11 from MIPAS spectra and validation is in preparation. A global map of CFC-11 at 275 hPa is shown in Fig. 8. The

standard error of the mean value within a latitude-longitude bin typically is around 5 pptv.

### 3 Southern hemispheric pollution belt

As we will discuss in the following, the enhanced southern hemispheric mixing ratios of tropospheric C<sub>2</sub>H<sub>6</sub> and O<sub>3</sub> are attributed to biomass burning in South America, Africa, Australia and Indonesia. For a similar period, MOPITT measured enhanced CO, which has also been attributed to biomass burning. The CO plume presented by Edwards et al. (2006) (their Fig. 1b) coincides nicely with the region of enhanced C<sub>2</sub>H<sub>6</sub>, PAN (Glatthor et al., 2007), and O<sub>3</sub> detected by MIPAS.

#### 3.1 Trajectory calculations

In order to assign the detected plume-like belt of polluted air to biomass burning, 12-day forward trajectories have been calculated with the HYSPLIT model (Draxler and Hess, 1997, 1998) (see also: <http://www.arl.noaa.gov/ready/hysplit4.html>), based on European Centre for Midrange Weather Forecast (ECMWF) analysis data. At the altitude range of interest, 12 days proved to be sufficient to capture intercontinental transport. Trajectory uncertainties are directionally unbiased for timescales larger than 5 h (Draxler, 1991) and thus are dominated by random errors, which in tendency cancel out when large ensembles are analysed statistically.

The trajectories were initialized at 4500 m altitude for southern African fires and at 2500 m altitude for South American, Indonesian and Australian fires. These trajectory altitudes comply with the so-called “injection altitude”, i.e. upper boundary of the mixing layer, which was found typical for biomass fires in these regions by Labonne et al. (2007). However, it should be mentioned that the final trajectory pattern varies only marginally with the injection altitude varying between 2500 and 4500 m. Burning areas were identified using daily Tropical Rainfall Measuring Mission (TRMM) Visible and Infrared Scanner (VIRS) satellite data (Giglio et al., 2000). As starting points of plume trajectories locations were selected where clusters of TRMM fire counts were found in the time interval 9 October 2003 to 12 November 2003, i.e. in the observation period of which data are presented here plus an 12-day extension towards earlier days to allow aged plume air to be detected. One trajectory represents approximately 10 fire counts.

Results of the trajectory calculations are shown in Fig. 9, where those parts of the trajectories are included which, during the averaging period, fall into the altitude range 7–11 km. Elevated C<sub>2</sub>H<sub>6</sub> over the South Atlantic, north of about 25° S can be attributed mainly to equatorial (15° S–10° N) American biomass burning, while further south the plume is formed both by equatorial and non-equatorial airmasses. Polluted

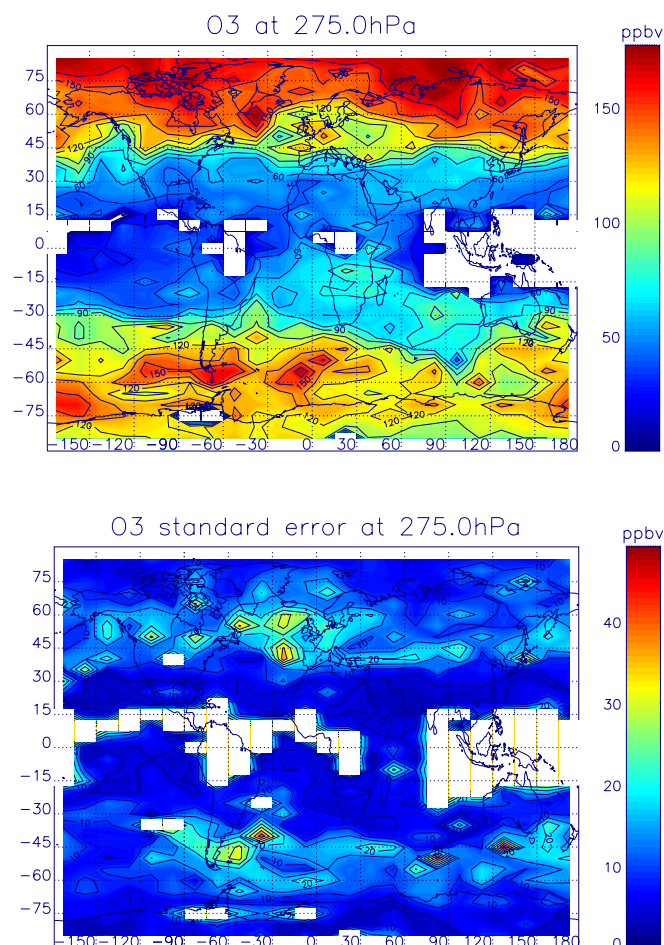


**Fig. 6.** VMR distribution of O<sub>3</sub> at 275 hPa, averaged from 21 October to 12 November 2003 (upper panel). Larger mixing ratios are found at northern and southern latitudes, where stratospheric air is sounded at this altitude. Enhanced tropospheric ozone is observed within the plume. The lower panel shows the standard error of the mean. Note the different colour scales. For more details, see Fig. 3.

air masses over Africa north of about 25° S are assigned to African vegetation burning. South of 25° S both African and South American airmasses contribute to the plume. Also the plume over the Indian Ocean is formed by airmasses of various origins, where African sources are predominant in the northern part of the plume.

#### 3.2 Plume tracer C<sub>2</sub>H<sub>6</sub>

The bulk of biomass burning plume trajectories, in particular those starting from tropical America and Africa, covers the same geolocations where enhanced C<sub>2</sub>H<sub>6</sub> is seen. C<sub>2</sub>H<sub>6</sub>, like other non-methane hydrocarbons, is generated by both flaming and smouldering combustion (Lobert and War-natz, 1993) but larger quantities are produced via smouldering combustion (Crutzen and Andreae, 1990). Its expected

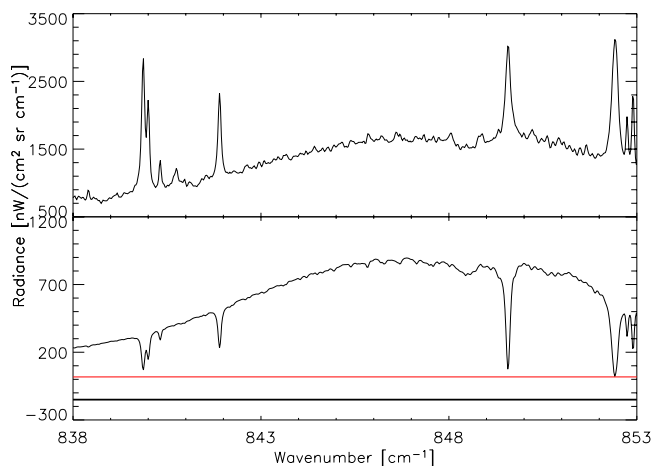


**Fig. 7.** MIPAS spectrum in the wavenumber range where CFC-11 is analysed. See Fig. 1 for details.

atmospheric lifetime in the upper troposphere is estimated at 100 days (Mauzerall et al., 1998), which is much longer than the episode under analysis. This suggests that, among the available MIPAS data, C<sub>2</sub>H<sub>6</sub> is a suitable tracer for plumes of polluted air. In order to define a threshold for plume air, the average value and the standard deviation of the C<sub>2</sub>H<sub>6</sub> mixing ratios of all tropical and southern hemispheric (i.e. 15° N to 90° S) 5° × 15° latitude-longitude bins not touched by any of the trajectories was calculated. The average (weighted by the inverse variance of the mean value of each bin) is 90 pptv and is understood to represent the southern hemispheric background mixing ratio at 275 hPa. The average plus two standard deviations is 221 pptv and is considered a suitable threshold for plume air (Fig. 10). This threshold reduces the one-sided risk that background air is misinterpreted as plume air, but does not minimize the complementary risk, i.e. that plume air parcels may remain undetected, in particular in the Pacific area, where presumably more divergent trajectories lead to smaller C<sub>2</sub>H<sub>6</sub> mixing ratios.

Certainly our analysis cannot exclude C<sub>2</sub>H<sub>6</sub>-loading from other sources than biomass burning. Industrial and megacity emissions could also contribute to enhanced C<sub>2</sub>H<sub>6</sub> mixing ratios. If these sources are situated in the vicinity or in the upwind region of vegetation fire events, they could contribute to the C<sub>2</sub>H<sub>6</sub> currently assigned to biomass burning. Analysis of MIPAS data recorded at other times than during the biomass burning season is planned and will help to identify other sources of upper tropospheric C<sub>2</sub>H<sub>6</sub> in the southern hemisphere. This issue seems particularly important to explain some of the data bins over the Pacific Ocean west of Colombia, Ecuador and Peru and is discussed in more depth in Sect. 3.5.

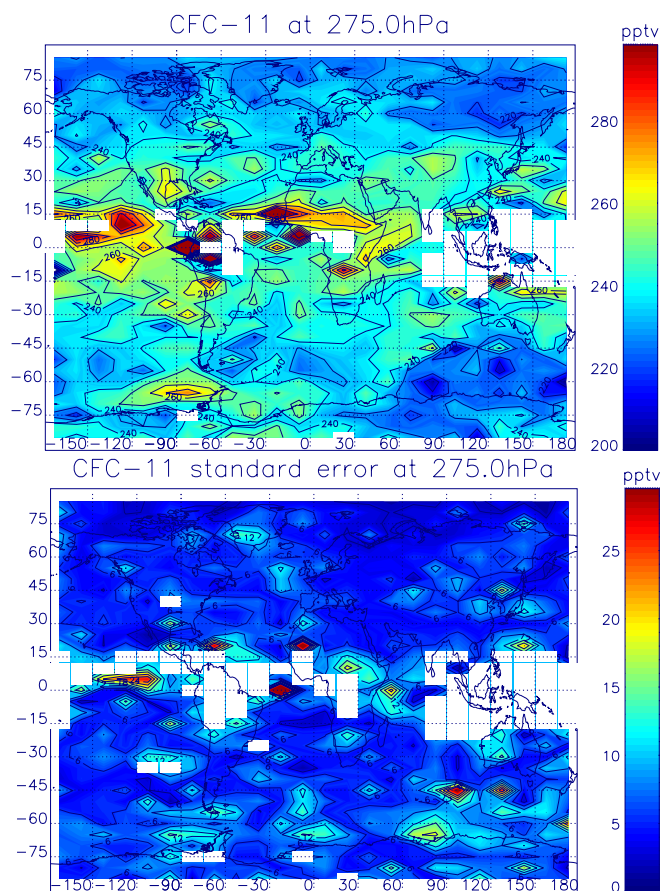


**Fig. 8.** VMR distribution of CFC-11 at 275 hPa, averaged from 21 October to 12 November 2003 (upper panel). Low values at high latitudes indicate stratospheric air sounded by MIPAS. Particularly high values near the equator most probably are artefacts due to extreme moisture or even undetected cloud signal in the spectra, to which the CFC-11 retrieval proves to be particularly sensitive. The lower panel shows the standard error of the mean. Note the different colour scales. For more details, see Fig. 3.

Figure 10 suggests that air polluted by equatorial American fires contains somewhat but not significantly more C<sub>2</sub>H<sub>6</sub> weighted by trajectory density than air parcels from other vegetation fires. By the term trajectory density we define the number of trajectories touching the bin times the residence time of the air parcel within the bin divided by the area of the bin. The mean ratio of C<sub>2</sub>H<sub>6</sub> mixing ratio over trajectory density is 10.1 ± 4.3 ppmv × km<sup>2</sup>/h for the Amazonian plume, while it is only 8.0 ± 2.4 ppmv × km<sup>2</sup>/h for the African plume. This ratio of about a factor of 1.26 is somewhat but not significantly lower than that one would expect from emission factors (gram species per kilogram of dry matter burned) presented by Andreae et al. (2001) who report values of 0.5 to 1.9 for tropical forest fires which is the dominating type of vegetation fires in equatorial America. These authors report

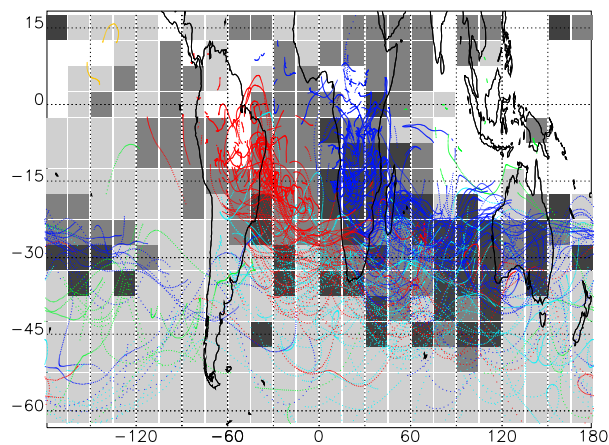


**Fig. 9.** Trajectories starting at geolocations of fire count clusters in the period from 13 October to 12 November 2003. Colour coding reflects the different starting points: blue=Africa, red=tropical America, yellow=north America, light blue=southernmost America, green=Australia and Indonesia. Only those points of the trajectories are shown which fall between 7 and 11 km, i.e. the measurement altitude plus/minus approximately half an altitude resolution of the MIPAS measurement. White background shading indicates data gaps due to clouds within the MIPAS field of view. Light grey corresponds to C<sub>2</sub>H<sub>6</sub> below 216 pptv and indicates air masses outside the plume. Dark grey and black is C<sub>2</sub>H<sub>6</sub> above 216 pptv and represents plume air. Regions within the plume where ozone is above 70 ppbv are shaded black. Obviously high ozone mixing ratios are not distributed equally over the plume.

a C<sub>2</sub>H<sub>6</sub> emission factor for savanna and grassland burning of only  $0.32 \pm 0.16$ . This difference is explained by the reduced completeness of combustion, which is significantly higher for the flaming combustion predominant in savanna burning than for the smouldering combustion more relevant in tropical rain forest burning (Jain et al., 2006). The different C<sub>2</sub>H<sub>6</sub> loading of polluted air has to be considered when this species is used as plume tracer in any quantitative way. This, however, is not a particular disadvantage of the species C<sub>2</sub>H<sub>6</sub> used as plume tracer here: The same caveat applies to the frequently used tracer CO, whose emission factors are also nearly a factor of two higher for rainforest burning than savanna and grassland fires (Andreae et al., 2001).

### 3.3 Ozone morphology within the plume

Ozone is an indirect biomass burning product whose main precursors include CO and NO<sub>x</sub>, which are both directly associated with biomass burning, and whose concentration critically depends on the level of NO<sub>x</sub>. MIPAS ozone observations vary considerably within the biomass burning plume. In particular, the part of the plume attributed mainly to African savanna fires contains much more ozone compared to the plume of equatorial American biomass burning where rain

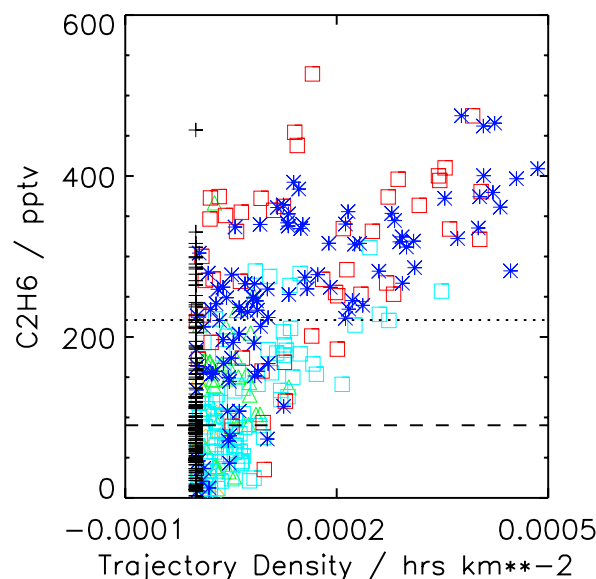


**Fig. 10.** C<sub>2</sub>H<sub>6</sub> VMR over trajectory density. Trajectory density is the number of trajectories starting at biomass burning areas which touch a  $5^\circ \times 15^\circ$  latitude-longitude bin, weighted by the time the trajectory is within the bin. The dashed line represents southern hemispheric background C<sub>2</sub>H<sub>6</sub>, the dotted line is the plume threshold. Coloured symbols represent plume air. The trajectory origin is colour-coded as in Fig. 9, i.e. light blue squares: subtropical South America; red squares: Equatorial South America; yellow diamonds: North America; dark blue asterisks: Africa; green triangles: Australia, Indonesia. Black crosses represent air outside the plume.

forest fires are prevailing. In turn, in the outflow region of equatorial American burning over the South Atlantic, no bins with ozone mixing ratios above 70 ppbv are observed except near the coast at about  $25^\circ$  S, where non-equatorial air-masses also contribute. O<sub>3</sub>/C<sub>2</sub>H<sub>6</sub> ratios were calculated for each bin inside the plume, where in case of ambiguous origin of air masses the bin was assigned to the source region whose trajectories predominated in terms of number of trajectories touching the bin times residence time of the air parcel within the bin (Fig. 11, upper panel). The mean O<sub>3</sub>/C<sub>2</sub>H<sub>6</sub> ratio is  $225 \pm 26$  in the African plume but only  $175 \pm 10$  in the Amazonian plume. In the Australian part of the plume high ozone values (above 100 ppbv) are observed, too, but these are attributed to stratospheric signal, as discussed below in Sect. 3.4. It should be noted that bins touched by trajectories from different origin do not necessarily hint at mixing in any physical sense. Instead, numerical mixing can be caused by averaging over the observation period in the case of a non-stationary windfield.

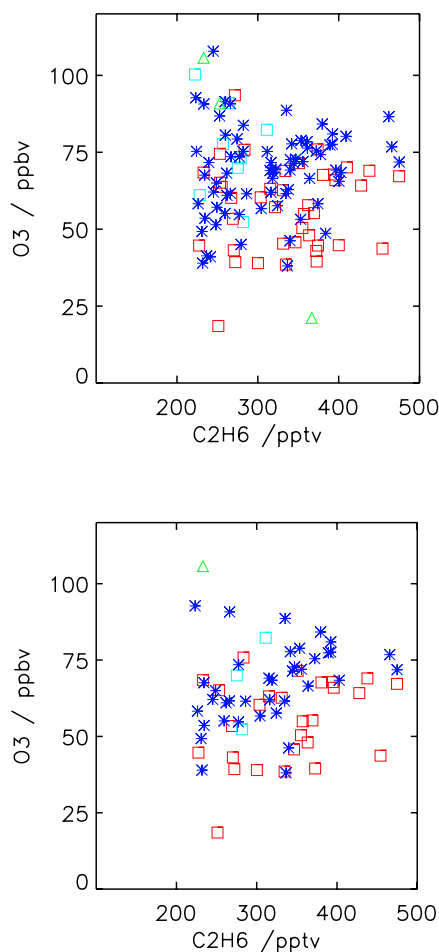


**Fig. 11.** O<sub>3</sub> – C<sub>2</sub>H<sub>6</sub> scatter plot. Colour coding as in Fig. 9. Upper panel: The O<sub>3</sub>/C<sub>2</sub>H<sub>6</sub> ratio in the African part of the plume (dark blue asterisks) is higher than that of the tropical American part (red squares). No clear ozone/ethane correlation is evident within the plume. Also the Australian/Indonesian part of the plume (green triangles) contains data points of high ozone. Lower panel: As above but data points with CFC-11 below 245 pptv, hinting at stratospheric signal, filtered out.

### 3.4 Removal of stratospheric signal

High ozone mixing ratios along with low C<sub>2</sub>H<sub>6</sub> values in the Australian part of the plume suggest that the ozone seen at 275 hPa might be affected by a stratospheric ozone signal. The ozone signal at this altitude can be contaminated by stratospheric ozone by two mechanisms of entirely different nature: Either stratospheric air could have been mixed or transported into the upper troposphere (c.f. Bremer et al., 2004); or, in the case of a low tropopause, due to the limited altitude resolution of the MIPAS ozone retrievals, stratospheric ozone could be misinterpreted as upper tropospheric ozone. In the given context, however, it is not necessary to

distinguish between either of these causes of stratospheric signal, since the effect would be the same: Stratospheric ozone would erroneously be attributed to a biomass burning plume. To determine data bins which are dominated by any of these potentially stratospheric ozone signals mentioned above, we use CFC-11 as a tracer. CFC-11 is a tropospheric species whose mixing ratios rapidly decrease with altitude in the stratosphere. Further, CFC-11 is long-lived and well-mixed in the troposphere and its mixing ratios are not driven by fire events. Its averaging kernels in the tropopause region are of similar width as those of ozone. Therefore, low CFC-11 values hint at a stratospheric ozone signal in the observed data bin.

Indeed some plume bins related to trajectories starting in Australia and extratropical southern America are characterized by low CFC-11 mixing ratios. This applies to data bins over the Pacific Ocean and the southern Atlantic east of southern Argentina and explains the high O<sub>3</sub>/C<sub>2</sub>H<sub>6</sub> ratios (green and light blue symbols in Fig. 11). Air parcels with CFC-11 mixing ratios below 245 pptv were rejected from further analysis. This particular threshold removed most of the spurious data points with high ozone and low C<sub>2</sub>H<sub>6</sub> mixing ratios which are attributed to stratospheric contamination. On the other hand, this threshold left enough data points for statistical analysis. Indeed the lower panel of Fig. 11, which shows the O<sub>3</sub>/C<sub>2</sub>H<sub>6</sub> ratios after application of the CFC-11 filter, includes much less data points with high (possibly stratospheric) ozone and low C<sub>2</sub>H<sub>6</sub> compared to the unfiltered scatter plot. Nevertheless, some suspicious data points with high O<sub>3</sub> and low C<sub>2</sub>H<sub>6</sub> remain even after application of the CFC-11 filter, which presumably is not sensitive enough to remove all stratospheric ozone signal. This sub-optimal behaviour of the CFC-11 filter is attributed to its application on bin averages without consideration of the typically nonlinear correlation of O<sub>3</sub> and CFC-11. Therefore, we restrict the further investigation of plume ozone to the tropical American and South African plumes. The contrast between the O<sub>3</sub>/C<sub>2</sub>H<sub>6</sub> ratios of the Amazonian and African plumes is not substantially changed through this data filter: After application of the filter the mean ratios are 214±27 for the African plume and 167±12 for the Amazonian one.

### 3.5 Discussion

Tropical rain forest fire emissions mostly occur near the inner tropic convergence zone and it is obvious that emitted gases can be rapidly transported to the altitudes of interest (i.e. seen by MIPAS) by convection (Greco et al., 1990; Andreae et al., 2001). For subtropical savanna fire emissions, the situation is not that clear because of predominant subsidence of air masses at these latitudes. Certainly, fires provide additional heating at the surface which enhances convection. Nevertheless, during convection colder ambient air is always mixed into the air parcel to be lifted and it is not quite clear, which altitudes can be reached. Chatfield et al. (2002) report

frequent final pollutant injection by cloud convection over southern Africa in September–October 1997. These authors mention both thunderstorm-scale venting as well as synoptic scale venting as mechanisms of uplifting of pyrogenic pollution. However, no pyrogenic deep convection has to our knowledge been reported for subtropical conditions with prevailing subsidence. Trentmann et al. (2006) state that the nature of pyro-convection is not fully understood, and Luderer et al. (2006) have shown that pyroconvection depends largely on the actual background meteorology. Another mechanism of uplifting pyrogenic pollution under the subsiding branch of the Hadley cell into the upper troposphere has been proposed by Andreae et al. (2001): The polluted air is transported into the tropics at lower levels and lofted there by deep convection. Typical uplifting mechanisms for African biomass burning plume air are discussed in Chatfield et al. (1998). The area where pyro-polluted air reaches higher altitudes was identified to be the Congo basin (c.f. Fig. 5e and f in their paper). In our study, we try to appropriately characterize the uplifting and transport process by starting the trajectory calculations at the so-called “injection altitude”, an altitude empirically determined by Labonne et al. (2007) and found consistent with the upper edge of the boundary layer. Tests have shown that the final trajectory pattern is quite robust against variation of the assumed injection altitude in a range from 2500 to 4500 m. Certainly, our approach misses any subsynoptic uplifting taking place above the mixing layer.

Different plume composition may be caused by different type of vegetation burning, different combustion stage, the actual meteorological conditions including illumination and uplifting mechanisms, aging in different chemical environments, mixing etc. The most probable explanation for the lower O<sub>3</sub>/C<sub>2</sub>H<sub>6</sub> ratio in the Amazonian plume is that rainforest fires with predominantly smouldering combustion emit more C<sub>2</sub>H<sub>6</sub> than African biomass burning, where flaming grassland and savanna fires are prevailing (Delmas et al., 1999). The use of C<sub>2</sub>H<sub>6</sub> mixing ratios to quantify the plume strength then leads to an overestimated Amazonian plume. The differences between equatorial American and African O<sub>3</sub>/C<sub>2</sub>H<sub>6</sub> ratios is fully consistent with the different ratios of C<sub>2</sub>H<sub>6</sub>/trajectory density and thus suggest equal ozone production efficiency in both plumes. Consideration of the different emission factors as reported by Andreae et al. (2001) may even suggest a more efficient ozone production on the Amazonian part of the plume. The higher ozone mixing ratios detected over Africa are attributed to higher trajectory densities.

Different residence time of pyro-polluted air in the lower troposphere with different prevailing chemistry is, apart from different pollutant source strengths of savanna versus rainforest and smouldering versus flaming combustion, a further candidate explanation of different mean O<sub>3</sub>/C<sub>2</sub>H<sub>6</sub> ratios. This would suggest that African savanna-fire pyro-polluted air resides longer in the lower troposphere compared

to its Amazonian counterpart. Long lower tropospheric residence times particularly of African pyro-polluted air have been reported by Edwards et al. (2006) and references therein. Furthermore, additional upper tropospheric ozone can also be produced by lightning-induced NO<sub>2</sub> and thus depends on thunderstorm activity along the actual trajectories (Staudt et al., 2002; Edwards et al., 2003). Indeed, at regions covered by trajectories associated with African biomass burning events there was higher thunderstorm activity in October and November 2003 than at those regions covered by trajectories started at equatorial American forest fires ([http://thunder.nsstc.nasa.gov/query/2003/2003\\_october.png](http://thunder.nsstc.nasa.gov/query/2003/2003_october.png) and [http://thunder.nsstc.nasa.gov/query/2003/2003\\_november.png](http://thunder.nsstc.nasa.gov/query/2003/2003_november.png)). No evidence for a relation between the mean age of the trajectories falling within a bin and the O<sub>3</sub> enhancement has been found.

Ziemke et al. (2006) (their Fig. 5b) inferred tropospheric ozone distributions from Aura OMI and MLS measurements, which show an O<sub>3</sub> plume extending from tropical America in October and November 2004. This either hints at different meteorological conditions or fire activity in 2003 versus 2004 (a significant interannual variation of CO emissions has been suggested by Gloudemans et al. (2006)) or may be attributed to the fact that their data represent the entire troposphere while MIPAS data represent the atmosphere above about 7 km.

The C<sub>2</sub>H<sub>6</sub> plume over the Pacific Ocean, west of Colombia, Ecuador and Peru deserves some further discussion, since in the altitude of region of interest (7–11 km) this region is only sparsely covered with trajectories starting at fire events. Possibly the uplifting processes are not correctly accounted for by the trajectory calculations. Another explanation would be urban outflow, e.g. from Mexico City or Panama City.

#### 4 Conclusions

Southern hemispheric C<sub>2</sub>H<sub>6</sub> generated by biomass burning reaches similar abundances as northern hemispheric enhancements. The MIPAS measurements of southern hemispheric C<sub>2</sub>H<sub>6</sub> nicely confirm the spatial extension of the biomass burning plume reported by Edwards et al. (2006) and complement the dataset published by these authors, by adding further information on the chemical composition of the plume. The particular advantage of a Fourier transform spectrometer like MIPAS is that it measures different species (here: C<sub>2</sub>H<sub>6</sub>, O<sub>3</sub>, and CFC-11) in the same air mass at similar altitude resolution, which allows a more straightforward interpretation compared to analysis of data products from different sensors which have different spatial resolution.

African and South American vegetation burning appears to be the major source of southern hemispheric upper tropospheric C<sub>2</sub>H<sub>6</sub> during the episode under analysis, since enhanced mixing ratios are confined to regions covered by

trajectories started above fire events. However, a signal of other anthropogenic pollution sources, e.g. from megacities or industrial plants (Talbot et al., 1996) in the vicinity of forest fires cannot be excluded. The source of enhanced C<sub>2</sub>H<sub>6</sub> over the Pacific Ocean, Galapagos area, is currently under investigation. At least at tropical latitudes where the possibility of contamination of the measured signal by a stratospheric contribution can safely be excluded, upper tropospheric ozone enhancements are confined to the pollution belt. Flaming combustion, which is prevailing in southern African fires, is seen on a hemispheric scale to contribute more efficiently to a high upper tropospheric O<sub>3</sub>/C<sub>2</sub>H<sub>6</sub> ratio than smouldering combustion which is typical for the Amazonian rain forest. This is explained by the larger C<sub>2</sub>H<sub>6</sub> emission factors of forest fires, which leads to an overestimation of the related plume strength. The final decision on whether the observed differences in ozone production are primarily driven by different trace gas loading in the plume through different types of combustion, or whether they are driven by different prevailing uplifting processes keeping the air in different chemical regimes remains somewhat speculative without the explicit consideration of small-scale convective processes in the trajectory calculation, even if the relevant chemical processes within the plume are modelled. Further studies on this and related questions will benefit from MIPAS measurements of further biomass-burning related species, particularly CO (Funke et al., 2007), PAN and C<sub>2</sub>H<sub>2</sub> (Glatthor et al., 2007), and H<sub>2</sub>CO (Steck et al., 2007a), which confirm the extension of the plume-like pollution belt in the southern hemisphere of 2003. C<sub>2</sub>H<sub>6</sub>/CO and C<sub>2</sub>H<sub>2</sub>/CO ratios can be used to distinguish between pollution from biomass burning and pollution from megacities (Talbot et al., 1996). More generally speaking, the availability of a series of primary and secondary pollutants can be used to better constrain modelling of the chemical processes within the plume.

Furthermore, the analysis of data recorded before and after the biomass burning season is planned in order to detect other sources of these pollutants, e.g. megacities and industrial plants. A possible improvement of the absolute accuracy of our C<sub>2</sub>H<sub>6</sub> retrievals by use of the most recent spectroscopic data will be investigated. Further studies will also include chemistry transport modelling based on the actual meteorological conditions as well as a comparison of the biomass burning season of different years. The data of this study are available to registered users via <http://www.fzk.de/imk/asf/ame/envisat-data/>.

**Acknowledgements.** The authors like to thank S. Chabrillat, S. Turquety, and an unknown reviewer for their insightful comments which have helped a lot to improve the paper. ESA has provided MIPAS Level-1B data. Meteorological analysis data used for retrieval calculations were provided by ECMWF. AL and TS have been funded by Helmholtz Gemeinschaft Deutscher Großforschungszentren under Virtual Institute IMACCO, contract number VH-VI-117. SK has been funded by BMBF under contract number 50 EE 0512.

Edited by: L. Carpenter

## References

- Andreae, M. O. and Merlet, P.: Emission of trace gases and aerosols from biomass burning, *G. Biogeochem. Cycles*, 15, 955–966, doi:10.1029/2000GB001382, 2001.
- Andreae, M. O., Artaxo, P., Fischer, H., Freitas, S. R., Grégoire, J.-M., Hansel, A., Hoor, P., Kormann, R., Krejci, R., Lange, L., Lelieveld, J., Lindinger, W., Longo, K., Peters, W., de Reus, M., Scheeren, B., Silva Dias, M. A. F., Ström, J., van Velthoven, P. F. J., and Williams, J.: Transport of biomass burning smoke to the upper troposphere by deep convection in the equatorial region, *Geophys. Res. Lett.*, 28, 951–954, 2001.
- Bremer, H., Kar, J., Drummond, J. R., Nichitu, F., Zou, J., Liu, J., Gille, J. C., Deeter, M. N., Francis, G., Ziskin, D., and Warner, J.: Spatial and temporal variation of MOPITT CO in Africa and South America: A comparison with SHADOZ ozone and MODIS aerosol, *J. Geophys. Res.*, 109, D12304, doi:10.1029/2003JD004234, 2004.
- Chatfield, R. B., Vastano, J. A., Li, L., Sachse, G. W., and Connors, V. S.: The Great African plume from biomass burning, in: Generalizations from a three-dimensional study of TRACE A carbon monoxide, *J. Geophys. Res.*, 103, 28 059–28 077, 1998.
- Chatfield, R. B., Guo, Z., Sachse, G. W., Blake, D. R., and Blake, N. J.: The subtropical global plume in the Pacific Exploratory Mission-Tropics A (PEM-Tropics A), PEM-Tropics B, and the Global Atmospheric Sampling Program (GASP): How tropical emissions affect the remote Pacific, *J. Geophys. Res.*, 4278, doi: 10.1029/2001/JD000497, 2002.
- Coheur, P., Herbin, H., Clerbaux, C., Hurtmans, D., Wespes, C., Carleer, M., Turquety, S., Rinsland, C. P., Remedios, J., Hauglustaine, D., Boone, C. D., and Bernath, P. F.: ACE-FTS observation of a young biomass burning plume: first reported measurements of C<sub>2</sub>H<sub>4</sub>, C<sub>3</sub>H<sub>6</sub>O, H<sub>2</sub>CO and PAN by infrared occultation from space, *Atmos. Chem. Phys.*, 7, 5437–5446, 2007, <http://www.atmos-chem-phys.net/7/5437/2007/>.
- Crutzen, P. J. and Andreae, M. O.: Biomass Burning in the Tropics, in: Impact on Atmospheric Chemistry and Biogeochemical Cycles, *Science*, 250, 1669–1678, 1990.
- Delmas, R. A., Druilhet, A., Cros, B., Durand, P., Delon, C., La-caux, J. P., Brustet, J. M., Serca, D., Affre, C., Guenther, A., Greenberg, J., Baugh, W., Harley, P., Klinger, L., Brasseur, P. G. G., Zimmerman, P. R., Grégoire, J. M., Janodet, E., Tournier, A., Perros, P., Marion, T., Gaudichet, A., Ruellan, H. C. S., Cautenet, P. M. S., Bouka Biona, D. P. C., Nganga, D., Tathy, J. P., Minga, A., Loemba-Ndembi, J., and Ceccato, P.: Experiment for Regional Sources and Sinks of Oxidants (EXPRESSO): An overview, *J. Geophys. Res.*, 104, 30 609–30 624, 1999.
- Draxler, R. R.: The accuracy of trajectories during ANATEX calculated using dynamic model analyses versus rawinsonde observations, *J. Appl. Meteorol.*, 30, 1446–1467, 1991.
- Draxler, R. R. and Hess, G. D.: Description of the HYSPLIT\_4 modeling system, NOAA Tech. Memo. ERL ARL-224, 24 pp., 1997.
- Draxler, R. R. and Hess, G. D.: An overview of the HYSPLIT\_4 modelling system for trajectories, dispersion and deposition,

- Aust. Meteorol. Mag., 47, 295–308, 1998.
- Edwards, D. P., Lamarque, J.-F., Attié, J.-L., Emmons, L. K., Richter, A., Cammas, J.-P., Gille, J. C., Francis, G. L., Deeter, M. N., Warner, J., Ziskin, D. C., Lyjak, L. V., Drummond, J. R., and Burrows, J. P.: Tropospheric ozone over the tropical Atlantic: A satellite perspective, *J. Geophys. Res.*, 108, 4237, doi:10.1029/2002JD002927, 2003.
- Edwards, D. P., Emmons, L. K., Gille, J. C., Chu, A., Attié, J.-L., Giglio, L., Wood, S. W., Haywood, J., Deeter, M. N., Massie, S. T., Ziskin, D. C., and Drummond, J. R.: Satellite-observed pollution from Southern Hemisphere biomass burning, *J. Geophys. Res.*, 111, D14312, doi:10.1029/2005JD006655, 2006.
- Fischer, H., Birk, M., Blom, C., Carli, B., Carlotti, M., von Clarmann, T., Delbouille, L., Dudhia, A., Ehhalt, D., Endemann, M., Flaud, J. M., Gessner, R., Kleinert, A., Koopmann, R., Langen, J., López-Puertas, M., Mosner, P., Nett, H., Oelhaf, H., Perron, G., Remedios, J., Ridolfi, M., Stiller, G., and Zander, R.: MIPAS: an instrument for atmospheric and climate research, *Atmos. Chem. Phys. Discuss.*, 7, 8795–8893, 2007, <http://www.atmos-chem-phys-discuss.net/7/8795/2007/>.
- Fishman, J., Wozniak, A. E., and Creilson, J. K.: Global distribution of tropospheric ozone from satellite measurements using the empirically corrected tropospheric ozone residual technique: Identification of the regional aspects of air pollution, *Atmos. Chem. Phys.*, 3, 893–907, 2003, <http://www.atmos-chem-phys.net/3/893/2003/>.
- Funke, B., López-Puertas, M., Bermejo-Pantaleón, D., von Clarmann, T., Stiller, G. P., Höpfner, M., Grabowski, U., and Kaufmann, M.: Analysis of nonlocal thermodynamic equilibrium CO 4.7 $\mu$ m fundamental, isotopic and hot band emissions measured by the Michelson Interferometer for Passive Atmospheric Sounding on Envisat, *J. Geophys. Res.*, 112, D11305, doi:10.1029/2006JD007933, 2007.
- Giglio, L., Kendall, J. D., and Tucker, C. J.: Remote sensing of fires with the TRMM VIRS, *Int. J. Remote Sens.*, 21, 203–207, 2000.
- Glatthor, N., von Clarmann, T., Fischer, H., Funke, B., Gil-López, S., Grabowski, U., Höpfner, M., Kellmann, S., Linden, A., López-Puertas, M., Mengistu Tsidu, G., Milz, M., Steck, T., Stiller, G. P., and Wang, D.-Y.: Retrieval of stratospheric ozone profiles from MIPAS/ENVISAT limb emission spectra: a sensitivity study, *Atmos. Chem. Phys.*, 6, 2767–2781, 2006, <http://www.atmos-chem-phys.net/6/2767/2006/>.
- Glatthor, N., von Clarmann, T., Fischer, H., Funke, B., Grabowski, U., Höpfner, M., Kellmann, S., Kiefer, M., Linden, A., Milz, M., Steck, T., and Stiller, G. P.: Global peroxyacetyl nitrate (PAN) retrieval in the upper troposphere from limb emission spectra of the Michelson Interferometer for Passive Atmospheric Sounding (MIPAS), *Atmos. Chem. Phys.*, 7, 2775–2787, 2007, <http://www.atmos-chem-phys.net/7/2775/2007/>.
- Gludemans, A. M. S., Krol, M. C., Meirink, J. F., de Laat, A. T. J., van der Werf, G. R., Schrijer, H., van den Broek, M. M. P., and Aben, I.: Evidence for long-range transport of carbon monoxide in the Southern Hemisphere from SCIAMACHY observations, *Geophys. Res. Lett.*, 33, L16807, doi:10.1029/2006GL02804, 2006.
- Greco, S., Swap, R., Garstang, M., Ulanski, S., Shipman, M., Harriss, R. C., Talbot, R., Andreae, M. O., and Artaxo, P.: Rainfall and surface kinematic condition over central Amazonia during ABLE-2A, *J. Geophys. Res.*, 95, 17 001–17 014, 1990.
- Jacquinet-Husson, N., Scott, N. A., Chédin, A., and Chursin, A. A.: The GEISA spectroscopic database system updated for IASI (direct radiative transfer modeling), *Atmos. Oceanic Opt.*, 16, 256–261, 2003.
- Jain, A. K., Tao, Z., Yang, X., Gillespie, C.: Estimates of global biomass burning emissions for reactive greenhouse gases (CO, NMHCs, and NO<sub>x</sub>) and CO<sub>2</sub>, *J. Geophys. Res.*, 111, D06304, doi:10.1029/2005JD006237, 2006.
- Labonne, M., Bréon, F., and Chevallier, F.: Injection height of biomass burning aerosols as seen from a spaceborne lidar, *Geophys. Res. Lett.*, 34, L11806, doi:10.1019/2007GL029311, 2007.
- Lobert, J. M. and Warnatz, J.: Emissions from the Combustion Process in Vegetation, in: *Fire in the Environment: The Ecological, Atmospheric, and Climatic Importance of Vegetation Fires*, edited by: Crutzen, P. J. and Goldammer, J. G., John Wiley and Sons Ltd, 15–51, 1993.
- Luderer, G., Trentmann, J., Winterrath, T., Textor, C., Herzog, M., Graf, H. F., and Andreae, M. O.: Modeling of biomass smoke injection into the lower stratosphere by a large forest fire (Part II): sensitivity studies, *Atmos. Chem. Phys.*, 6, 5261–5277, 2006, <http://www.atmos-chem-phys.net/6/5261/2006/>.
- Mauzerall, D. L., Logan, J. A., Jacob, D. J., Anderson, B. E., Blake, D. R., Bradshaw, J. D., Heikes, B., Sachse, G. W., Singh, H., and Talbot, B.: Photochemistry in biomass burning plumes and implications for tropospheric ozone over the tropical South Atlantic, *J. Geophys. Res.*, 103, 8401–8423, 1998.
- Nett, H., Carli, B., Carlotti, M., Dudhia, A., Fischer, H., Flaud, J.-M., Perron, G., Raspollini, P., and Ridolfi, M.: MIPAS Ground Processor and Data Products, in: *Proc. IEEE 1999 International Geoscience and Remote Sensing Symposium*, 28 June–2 July 1999, Hamburg, Germany, 1692–1696, 1999.
- Norton, H. and Beer, R.: New apodizing functions for Fourier spectrometry, *J. Opt. Soc. Am.*, 66, 259–264, (Errata *J. Opt. Soc. Am.*, 67, 419, 1977), 1976.
- Rinsland, C. P., Dufour, G., Boone, C., Bernath, P., and Chiou, L.: Atmospheric Chemistry Experiment (ACE) measurements of elevated Southern Hemisphere upper tropospheric CO, C<sub>2</sub>H<sub>6</sub>, HCN, and C<sub>2</sub>H<sub>2</sub> mixing ratios from biomass burning emissions and long-range transport, *Geophys. Res. Lett.*, 32, L20803, doi:10.1029/2005GL024214, 2005.
- Rodgers, C. D.: *Inverse Methods for Atmospheric Sounding: Theory and Practice*, World Scientific, 2000.
- Rothman, L. S., Barbe, A., Benner, D. C., Brown, L. R., Camy-Peyret, C., Carleer, M. R., Chance, K., Clerbaux, C., Dana, V., Devi, V. M., Fayt, A., Flaud, J.-M., Gamache, R. R., Goldman, A., Jacquemart, D., Jucks, K. W., Lafferty, W. J., Mandin, J.-Y., Massie, S. T., Nemtchinov, V., Newnham, D. A., Perrin, A., Rinsland, C. P., Schroeder, J., Smith, K. M., Smith, M. A. H., Tang, K., Toth, R. A., Vander Auwera, J., Varanasi, P., and Yoshino, K.: The HITRAN molecular spectroscopic database: edition of 2000 including updates through 2001, *J. Quant. Spectrosc. Radiat. Transfer*, 82, 5–44, doi:10.1016/S0022-4073(03)00146-8, 2003.
- Spang, R., Remedios, J. J., and Barkley, M. P.: Colour indices for the detection and differentiation of cloud types in infra-red limb emission spectra, *Adv. Space Res.*, 33, 1041–1047, 2004.
- Staudt, A. C., Jacob, D. J., Logan, J. A., Bacchiocchi, D., Krishnamurti, T. N., and Poisson, N.: Global chemical model analysis of biomass burning and lightning influences over the South

- Pacific in austral spring, *J. Geophys. Res.*, 107(D14), 4200, doi: 10.1029/2000JD000296, 2002.
- Steck, T., Glatthor, N., von Clarmann, T., Fischer, H., Funke, B., Grabowski, U., Höpfner, M., Kellmann, S., Linden, A., Perrin, A., and Stiller, G. P.: Retrieval of global upper tropospheric formaldehyde H<sub>2</sub>CO distributions from high-resolution MIPAS-Envisat spectra, *Atmos. Chem. Phys. Discuss.*, 7, 13 627–13 652, 2007a.
- Steck, T., von Clarmann, T., Fischer, H., Funke, B., Glatthor, N., Grabowski, U., Höpfner, M., Kellmann, S., Kiefer, M., Linden, A., Milz, M., Stiller, G. P., Wang, D. Y., Allaart, M., Blumenstock, T., von der Gathen, P., Hansen, G., Hase, F., Hochschild, G., Kopp, G., Kyrö, E., Oelhaf, H., Raffalski, U., Redondas Marrero, A., Remsberg, E., Russell III, J., Stebel, K., Steinbrecht, W., Wetzell, G., Yela, M., and Zhang, G.: Bias determination and precision validation of ozone profiles from MIPAS-Envisat retrieved with the IMK-IAA processor, *Atmos. Chem. Phys.*, 7, 3639–3662, 2007b.
- Talbot, R. W., Bradshaw, J. D., Sandholm, S. T., Smyth, S., Blake, D. R., Blake, N. R., Sachse, G. W., Collins, J. E., Heikes, B. G., Anderson, B. E., Gregory, G. L., Singh, H. B., Lefter, B. L., and Bachmeier, A. S.: Chemical characteristics of continental outflow over the tropical South Atlantic Ocean from Brazil and Africa, *J. Geophys. Res.*, 101, 24 187–24 202, 1996.
- Trentmann, J., Luderer, G., Winterrath, T., Fromm, M. D., Textor, C., Herzog, M., Graf, H. F., and Andreae, M. O.: Modeling of biomass smoke injection into the lower stratosphere by a large forest fire (Part I): reference simulation, *Atmos. Chem. Phys.*, 6, 5247–5260, 2006.
- Vander Auwerra, J., Moazzen-Ahmadi, N., and Flaud, J.: Toward an accurate database for the 12 μm region of the ethane spectrum, *Astrophys. J.*, 662, 750–757, 2007.
- von Clarmann, T., Glatthor, N., Grabowski, U., Höpfner, M., Kellmann, S., Kiefer, M., Linden, A., Mengistu Tsidu, G., Milz, M., Steck, T., Stiller, G. P., Wang, D. Y., Fischer, H., Funke, B., Gil-López, S., and López-Puertas, M.: Retrieval of temperature and tangent altitude pointing from limb emission spectra recorded from space by the Michelson Interferometer for Passive Atmospheric Sounding (MIPAS), *J. Geophys. Res.*, 108, 4736, doi:10.1029/2003JD003602, 2003.
- Ziemke, J. R., Chandra, S., Duncan, B. N., Froidevaux, L., Bharatia, P. K., Levelt, P. F., and Waters, J. W.: Tropospheric ozone determined from Aura OMI and MLS: Evaluation of measurements and comparison with the Global Modeling Initiative's Chemical Transport Model, *J. Geophys. Res.*, 111, D19303, doi: 10.1029/2006JD007089, 2006.